# AMS study of the Pont-de-Montvert–Borne porphyritic granite pluton (French Massif Central) and its tectonic implications

Jean-Yves Talbot, Yan Chen, Michel Faure, Wei Lin

*Geophys. J. Int.* (2000) **140,** 677–686

# AMS study of the Pont-de-Montvert–Borne porphyritic granite pluton (French Massif Central) and its tectonic implications

Jean-Yves Talbot, Yan Chen, Michel Faure and Wei Lin
*UMR* 6530, *Université d'Orléans, France,* 45067 *Orléans Cedex* 2 *France. E-mail: yan.chen@uni-orleans.fr*

Accepted 1999 November 10. Received 1999 November 9; in original form 1998 November 11

## SUMMARY

Thermomagnetic experiments, isothermal remanent magnetization (IRM), hysteresis loops, X-ray reflection analyses, optic microscopic observations, bulk magnetic susceptibility and natural remanent magnetization (NRM) show that the susceptibility signal of 56 sites in the Pont-de-Montvert–Borne pluton is derived mostly from biotite with a very small proportion of ferromagnetic material. Low anisotropy degree (*P* parameter) and consistent AMS orientations among monzonite, enclaves and aplitic dykes indicate that the AMS was acquired during pluton emplacement in the subsolidus phase. Magnetic fabrics demonstrate that linear deformation is prominent in the area where the granite is in direct contact with micaschists, and that planar deformation becomes more important in the area where the pluton is surrounded by non-porphyritic peraluminous granites. AMS measurements also show that shallow plunging E–W-stretching lineations are the dominant structure over most of the studied area. Foliation orientations follow the pluton contour in the western part, indicating that the Pont-de-Montvert–Borne pluton is probably rooted in the west and extruded towards the east. These AMS results agree to some extent with fabric inferred from mineral preferred orientation. The AMS data support an E–W extensional tectonic setting during the Pont-de-Montvert–Borne pluton emplacement, which resulted from the Late Carboniferous crustal thinning of the Hercynian orogeny.

**Key words:** AMS, French Massif Central, Hercynian Belt, pluton emplacement.

## INTRODUCTION

It is already well established that the development of planar and linear fabrics in plutons is controlled by both magma crystallization dynamics and the regional stress field. Therefore, the structure of a pluton provides significant information on the regional tectonics. The role of granitic plutons as markers of the late stage of the orogenic evolution of the Hercynian Belt in the French Massif Central has recently been pointed out (e.g. Faure & Pons 1991; Faure 1995). One difficulty in the study of granite fabrics lies in measuring the planar and linear mineral preferred orientations, especially if the deformation is weak. Such studies generally involve time-consuming techniques using a universal stage (Marre 1982). An alternative method is to analyse the anisotropy of magnetic susceptibility (AMS) (Graham 1954). This method helps the mechanisms of pluton emplacement to be better understood, as has been demonstrated for several granitic plutons (e.g. Khan 1962; Ellwood & Whitney 1980; Bouchez *et al.* 1990; Rochette *et al.* 1992).

AMS analyses are applied here to the Pont-de-Montvert–Borne monzonitic pluton in the southeastern part of the French Massif Central. The Pont-de-Montvert–Borne pluton, which intruded the Cévennes micaschist during the Middle Late Carboniferous, is a syntectonic pluton. As shown by the kinematic indicators in the pluton aureole (sigmoidal quartz veins, shear bands, boudinaged andalousite, sigmoidal biotite or quartz pressure shadows around contact minerals), the pluton terminations are characterized by top-to-the-east and top-to-the-west shearing at the eastern and western terminations, respectively (Faure *et al.* 1992). Along the northern and southern contacts, coaxial flow predominates where mineral fabrics have already been analysed by means of field and universal stage, but with controversial interpretations (Fernandez 1977; Mialhe 1980; Faure *et al.* 1992). Fernandez (1977) and Mialhe (1980) used the K-feldspar megacryst subfabrics to determine the structure of the Pont-de-Montvert and Borne massifs, respectively. The N–S orientation of K-feldspar, and the planar deformation which generally follows the contour of the pluton with a principal E–W orientation led these authors to conclude that these plutons were intruded during N–S extensional tectonics. They further suggested that the pluton is of tabular shape dipping 40° to 50° north. In contrast, Faure *et al.* (1992)

argued that this technique is not suitable for studying the tectonic structure of granitic plutons. Based on field observations of enclaves, aplite dykes and cleavage of biotite and plagioclase, they found that the planar structure shows the same orientation as determined by Fernandez (1977) and Mialhe (1980); however, the linear structure is subhorizontal E–W trending, indicating an E–W stretching. Faure *et al.* (1992) suggested, moreover, that the monzonite-micaschist contact should incline towards the south in the south flank and towards the north in the north of the pluton.

In light of these uncertainties, an AMS study was undertaken to assess the fabric elements in the pluton. The origin of AMS is discussed in terms of magnetic mineralogy and granite rheology. Both conventional petrofabric and AMS techniques are compared and are used to constrain the tectonic setting and emplacement mechanism of the Pont-de-Montvert–Borne pluton.

## GEOLOGICAL SETTING

The French Massif Central comprises a large area, geologically related to the Hercynian orogeny, which formed during the Palaeozoic Gondwana–Laurussia collision (e.g. Matte 1986, and references therein). The French Massif Central records several tectonic metamorphic and magmatic events that took place between the Silurian and the Late Carboniferous (see Faure *et al.* 1999 for a recent review and references). In the northern part of the Massif, compression ended in the Late Devonian to Early Carboniferous ($\approx$360–350 Ma), whereas it lasted up to the Middle Carboniferous ($\approx$330 Ma) in the south. The entire massif experienced extensional tectonics during the Middle to Late Carboniferous ($\approx$320–300 Ma), again with extension beginning earlier in the north than in the south (Faure 1995). The Cévennes area forms the southeastern part of the French Massif Central (Fig. 1). It consists of a wide micaschist-quartzite series that experienced a prograde greenschist to lower amphibolite facies metamorphism (Rakib 1996). The flat-lying foliation and N–S- to NE–SW-trending stretching lineation (L1) is related to southward nappe-stacking during the Hercynian orogeny (Mattauer & Etchecopar 1976; Matte 1986; Faure *et al.* 1999). The metamorphism is dated at around 340 Ma using $^{40}Ar/^{39}Ar$ on biotite and muscovite (Caron 1994; Monié *et al.* 1999). After southward thrusting, the Cévennes micaschists experienced another ductile deformation characterized by E–W to NW–SE stretching lineations (L2). The early compressional foliation is cut by low-angle shear bands often associated with sigmoidal quartz veins, related to a late orogenic extensional stage of Middle–Late Carboniferous age (Faure 1995). The shear criteria indicate a top-to-the-east motion of the hanging wall.

The metamorphic sequence in the Cévennes is intruded in the north and south by the Mont-Lozère and Aigoual-St-Guiral-Liron plutons, respectively (Fig. 1). The Mont-Lozère massif shows several petrographic facies (Van Moort 1966). The non-porphyritic peraluminous Signaux granite and the porphyritic Pont-de-Montvert monzonite form the main parts of the massif. The Borne massif lies in the eastern part of the porphyritic monzonite and was left-laterally offset by the N–S-striking Villefort fault in the Late Permian (Fig. 1). Here, the Pont-de-Montvert and Borne massifs are treated as an single entity. Available Rb-Sr ages of the Pont-de-Montvert–Borne and the Signaux massifs range from 280 to 315 Ma. This last age is geologically the most acceptable (see discussion in Faure 1995). Recently, U-Pb measurements on zircon and monazite from these bodies yielded emplacement ages of around 320–315 Ma (Lancelot, personal communication). Biotite and muscovite $^{40}Ar/^{39}Ar$ ages from granite and hornfels range from 314 to 304 Ma (P. Monié, work in progress). These younger ages attest to a partial re-opening of the isotopic system related to a perigranitic hydrothermal event responsible for gold mineralization (Charonnat *et al.* 1997).

Owing to abundant structural indicators such as schlieren, enclaves, aplitic joints and mineral preferred orientation, the structure of the Pont-de-Montvert–Borne pluton has been extensively investigated (Fernandez 1977; Mialhe 1980; Faure *et al.* 1992). Weakly developed mineral fabrics and the lack of mylonites have led to differing interpretations. For example, according to Fernandez (1977), the Pont-de-Montvert–Borne pluton exhibits a submeridian mineral lineation, whereas Faure *et al.* (1992) describe a consistent E–W-trending lineation.

## SAMPLING

About 350 orientated cores were collected with a portable gasoline drill from 56 sites widely distributed in the Pont-Montvert–Borne pluton (Fig. 1). Five to 10 cores of several centimetres in length and 2.5 cm in diameter have been sampled from each site, over a surface area of more than 10 $m^2$. Most of the sites lie near the pluton boundaries, with fewer from the central part. The collection is composed mainly of monzonite with less than 10 per cent of aplite and enclave rocks. The cores were orientated, when it was possible, by both magnetic and sun compasses. The mean difference between magnetic and sun measurements was less than 0.5°.

## LABORATORY MEASUREMENTS

Before AMS measurements were taken, several methods were employed to identify the magnetic carriers. A thermomagnetic experiment was carried out to determine the Curie temperatures using CS3 apparatus and a KLY3 kappabridge. Magnetic susceptibility falls significantly at about 580 °C, which indicates the presence of magnetite (Fig. 2). A minor residual signal above 580 °C could be an indication of haematite (Fig. 2). The isothermal remanent magnetization (IRM) was measured on several representative specimens using an IM30 impulse magnetizer and a JR5 spinner magnetometer (Fig. 3). IRM acquisition increases rather rapidly at weak applied magnetic fields up to 150 mT, and then slows down thereafter. The specimens are not saturated by 1.0 T (Fig. 3). The IRM curves suggest the probable presence of ferromagnetic minerals; however, their concentration should not be important as the highest IRM intensity does not exceed $7 \times 10^{-2}$ A $m^{-1}$ for standard-size samples (Fig. 3).

X-ray reflection analyses on a Philips diffractometer with a Cobalt tube, and microscopic observations were obtained before defining the principal magnetic susceptibility carriers. Fig. 4 shows one of the X-ray reflection analyses, which indicates that the main minerals are quartz, K-feldspar, plagioclase (anorthite, albite) and biotite (annite), with a very small proportion of opaque minerals (haematite). Optical observations from several thin sections confirm the X-ray studies, in agreement with previous petrographic studies (Van Moort 1966; Mialhe 1980).

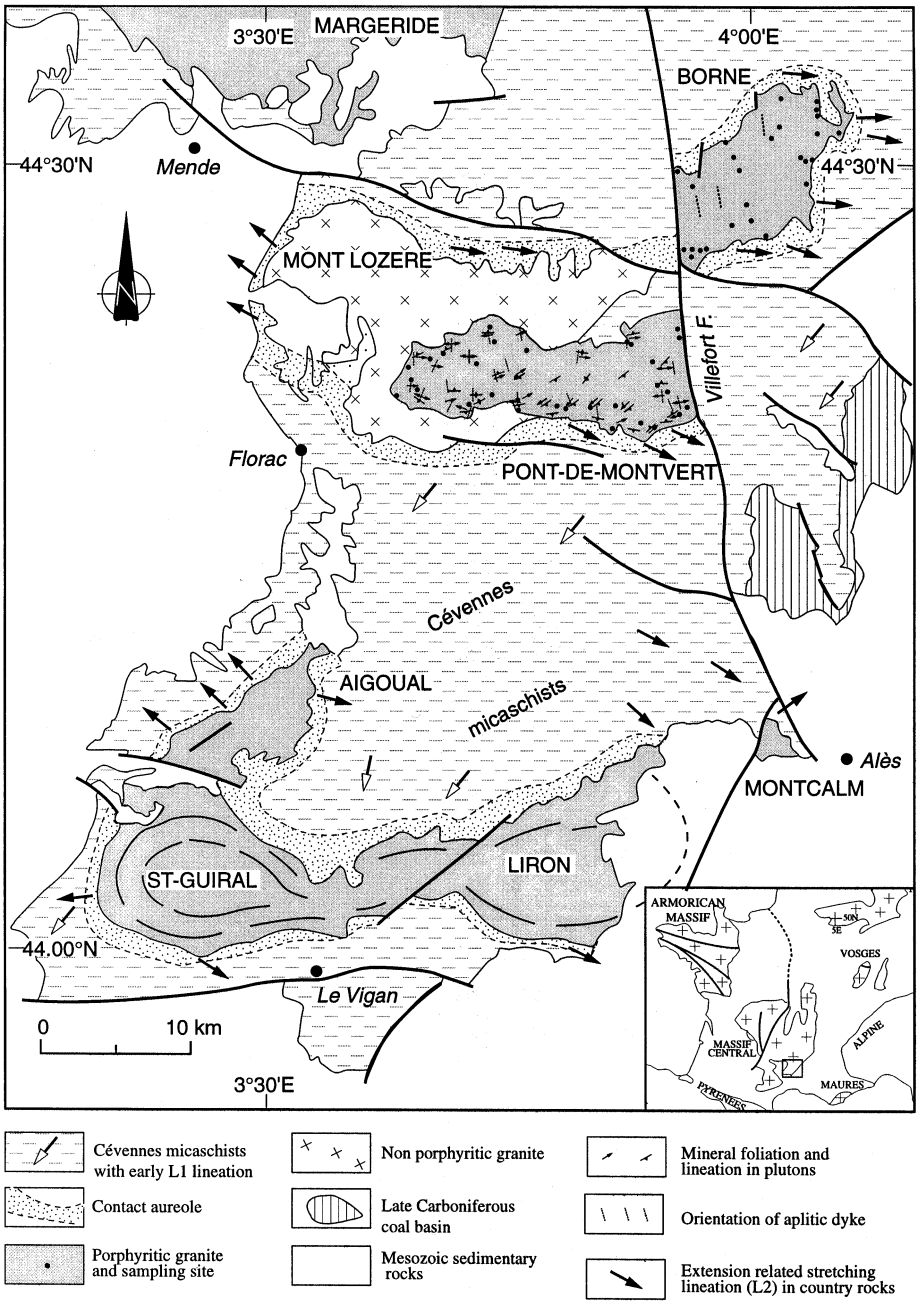


**Figure 1.** Structural map of the Cévennes area, showing the granitic massifs. Fabric elements in the Pont-de-Montvert–Borne pluton are according to Faure *et al.* (1992). The inset shows the study area in the French Palaeozoic massifs.

Hysteresis loops of some samples were also determined using a translation inductometer within an electromagnet providing a field of up to 1.0 T at the Palaeomagnetic Laboratory of Saint Maur (Paris). A strong dominant effect of the paramagnetic minerals is evidenced by the almost perfectly linear superimposition of the two curves produced during increasing and decreasing magnetic fields (Fig. 5). The paramagnetic susceptibility is about $10^{-9}\,m^3\,kg^{-1}$, and the saturation remanent magnetization is very weak ($\approx 10^{-4}\,A\,m^2\,kg^{-1}$), confirming that the ferromagnetic minerals are in very small proportion relative to the other minerals in the samples.

The bulk magnetic susceptibility (BMS) was measured with a KLY3 kappabridge. The histogram of the BMS intensity (Fig. 6a) shows a monomodal asymmetric distribution, ranging from 10 to $600 \times 10^{-6}$ SI and averaging $140 \pm 60 \times 10^{-6}$ SI. Enclaves possess magnetic susceptibilities slightly higher than those of the granites and aplites. The low BMS possibly indicates an abundance of paramagnetic material, with little magnetite. The range of values is compatible with that of paramagnetic minerals such as biotite (Tarling & Hrouda 1993), which are the main paramagnetic mineral components in these rocks.

The natural remanent magnetization (NRM) of each specimen was also measured on a JR5 spinner magnetometer. The NRM (Fig. 6b) has a relatively narrow range of asymmetrically distributed intensities from 0 to $26 \times 10^{-4}\,A\,m^{-1}$

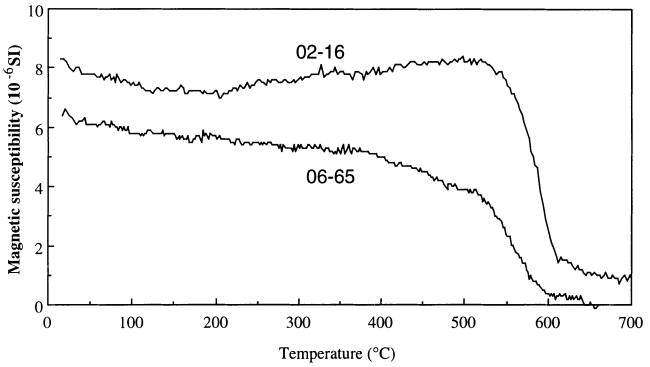


**Figure 2.** Thermomagnetic curves in air. The rapid decrease of magnetic susceptibility at about 580 °C and 630 °C indicates the existence of ferromagnetic minerals.

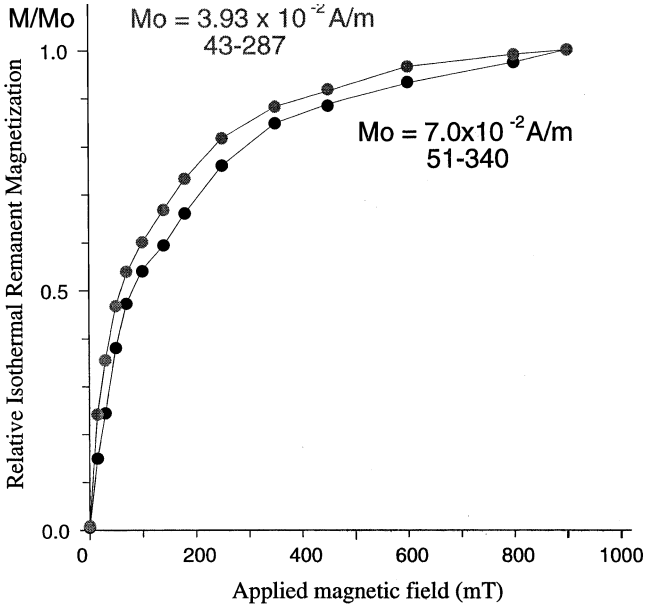


**Figure 3.** Acquisition of isothermal remanent magnetization, showing partial magnetic saturation with weak IRM intensity.

with a weak average of $6.4 \pm 5.6 \times 10^{-4}$ A m$^{-1}$. The weak value and narrow range of NRM may indicate that the sampled rocks are of 'non-magnetic' granite and relatively homogenous in their magnetic mineralogy (Ellwood & Wenner 1981).

## MEASUREMENTS OF THE ANISOTROPY OF MAGNETIC SUSCEPTIBILITY

AMS measurements were carried out on 377 specimens from 56 sites with a KLY3 kappabridge of $\approx 10^{-9}$ SI sensitivity. The three principal axes of the magnetic susceptibility ellipsoid ($K_{max} \geq K_{int} \geq K_{min}$) are denoted by squares, triangles and circles, respectively, in Fig. 7 (see also Table 1). For each site, the spatial distribution of these three axes has been defined by declination (Dec), inclination (Inc), precision parameters ($k_{max}$ and $k_{min}$) and confidence intervals at the 95 per cent level ($\alpha_{95max}$ and $\alpha_{95min}$; Table 1; Bingham 1964). Fig. 7 gives the stereographic distribution of the three principal magnetic fabric axes of each sample for each site. Within each site, $K_{max}$ is generally well grouped with E–W declinations and sub-horizontal ($<30°$) inclinations, especially for the sites in the Borne massif and the eastern part of the Pont-de-Montvert massif, where the pluton is not surrounded by non-porphyritic peraluminous granite (e.g. sites 14, 29). Otherwise, in the western part of the Pont-de-Montvert pluton, where the massif is in contact with non-porphyritic peraluminous granite, $K_{min}$ is better grouped, while $K_{max}$ and $K_{int}$ are more mixed (e.g. sites 41, 42, 53). The planar anisotropy is locally more pronounced than the linear one but its orientation varies with respect to its location in the pluton (Fig. 7). The foliation plunges towards the margins of the massif near the southern and western border (e.g. sites 38, 41, 56, 53 in Fig. 7). The plunge angles of foliation are also variable with respect to the border, being steeper in the south (40° to 50°) than in the north (10° to 20°).

## DISCUSSION AND CONLUSIONS

The magnetic mineralogical experiments show that the specimens possess low NRM intensities (average $= 6.4 \pm 5.6 \times 10^{-4}$ A m$^{-1}$). The weak bulk magnetic susceptibilities (average $= 1.4 \pm 0.65 \times 10^{-4}$ SI) fall in the 'non-magnetic' granite category (Ellwood & Wenner 1981), in which biotite normally carries the paramagnetic signal (Borradaile *et al.* 1987; Zapletal 1990). Thermomagnetic and IRM experiments indicate the existence of ferromagnetic minerals, but the magnetic susceptibility and remanence level are very low (Figs 2 and 3). X-ray reflection analyses and optic microscopic observations show that the modal mineral assemblage is composed of quartz, biotite, K-feldspar and plagioclase with very little opaque mineral content (Fig. 4). Thus, the ferromagnetic mineral concentration should be very low with only a minor influence on the AMS measurements.

Two parameters were computed to describe the shape and intensity of the magnetic susceptibility tensor. The first is the ellipsoid shape parameter ($T$) (Jelinek 1981; Hrouda 1982; see Table 1 for its formula), which varies from $-1$ (prolate) to $+1$ (oblate), and the second is the anisotropy degree ($P$), which relates to the fabric intensity (Jelinek 1981; see Table 1 for its formula). Most of the sites possess negative $T$-values, indicating that linear deformation is dominant (Table 1 and Fig. 8). In this study, $P$-values are low, ranging from 1.01 to 1.07 (Table 1 and Fig. 8). Interestingly, several samples collected from enclaves and aplites show similar AMS orientations (sites 06, 08 and 44 in Fig. 7).

One of the most interesting aspects of the application of magnetic fabrics is a new understanding of the mechanisms leading to fabric development in magmatic rocks. In the plutonic rocks where emplacement occurred through magma flow, the magnetic anisotropy is generally characterized by low values, less than 10 per cent (Hargraves *et al.* 1991). Thus, it is important to know if the observed fabrics were acquired during magmatic flow before granite crystallization, during pluton emplacement in the subsolidus stage, or during a late tectonic stage after emplacement and cooling. In this study, this last possibility is ruled out because the deformation magnitude ($P$ parameter) is weak, ranging from 1.01 to 1.07 (Fig. 8 and Table 1) with an average of $1.04 \pm 0.01$. This range of values indicates that the magnetic fabrics were not obtained after pluton emplacement (Hrouda & Chlupacova 1980; King 1966). Consequently, in spite of the presence of some important

**Table 1.** Summary of the principal results of the AMS measurements. *N*: number of measured specimens; Dec, Inc, $k_{max}$, $k_{min}$, $\alpha_{95min}$ and $\alpha_{95max}$: declination, inclination, Bingham (1964) bimodal statistics data; $K_{max}$, $K_{int}$, $K_{min}$: principal axes of the magnetic fabric; *P*: corrected anisotropy degree*; T: ellipsoid shape parameter†.

| Site | *N* | $K_{max}$ | | | | | | $K_{min}$ | | | | | | *P* | T |
|---|---|---|---|---|---|---|---|---|---|---|---|---|---|---|---|
| | | Dec (°) | Inc (°) | $k_{max}$ | $k_{min}$ | $\alpha_{95min}$ (°) | $\alpha_{95max}$ (°) | Dec (°) | Inc (°) | $k_{max}$ | $k_{min}$ | $\alpha_{95min}$ (°) | $\alpha_{95max}$ (°) | | |
| 1 | 11 | 274.7 | 5.4 | 45 | 33 | 6.3 | 7.3 | 21.3 | 69.5 | 31 | 4 | 7.5 | 19.6 | 1.045 | −0.428 |
| 2 | 9 | 263.5 | 8.1 | 308 | 38 | 2.7 | 7.5 | 22.4 | 73.3 | 129 | 6 | 4.1 | 18.2 | 1.041 | −0.379 |
| 3 | 11 | 263.9 | 6.3 | 95 | 43 | 4.3 | 6.4 | 42.0 | 82.0 | 76 | 8 | 4.8 | 14.6 | 1.038 | −0.445 |
| 4 | 13 | 268.7 | 10.0 | 100 | 25 | 3.9 | 7.7 | 3.8 | 33.1 | 26 | 1 | 7.5 | 28.8 | 1.046 | −0.36 |
| 5 | 19 | 89.0 | 2.8 | 111 | 42 | 3.0 | 4.9 | 354.6 | 58.8 | 53 | 10 | 4.4 | 9.9 | 1.053 | −0.315 |
| 6 | 16 | 266.9 | 8.7 | 60 | 12 | 4.5 | 10.0 | 357.5 | 38.7 | 21 | 2 | 7.6 | 22.6 | 1.038 | −0.537 |
| 7 | 9 | 261.3 | 5.7 | 75 | 47 | 5.4 | 6.8 | 148.4 | 66.8 | 73 | 3 | 5.5 | 26.2 | 1.039 | −0.482 |
| 8 | 10 | 85.2 | 4.7 | 77 | 37 | 5.0 | 7.3 | 190.7 | 72.0 | 59 | 7 | 5.7 | 15.7 | 1.041 | −0.225 |
| 9 | 4 | 265.2 | 11.0 | 29 | 5 | 12.8 | 29.5 | 357.8 | 65.1 | 3337 | 80 | 1.4 | 9.0 | 1.032 | −0.474 |
| 10 | 10 | 87.1 | 3.8 | 138 | 17 | 3.8 | 10.7 | 292.0 | 83.4 | 63 | 4 | 5.6 | 20.6 | 1.047 | −0.287 |
| 11 | 11 | 252.1 | 1.7 | 27 | 11 | 8.0 | 12.7 | 161.6 | 60.1 | 13 | 8 | 11.5 | 14.4 | 1.037 | 0.107 |
| 12 | 5 | 255.1 | 2.3 | 191 | 46 | 4.5 | 9.2 | 350.5 | 58.3 | 78 | 2 | 7.1 | 41.5 | 1.026 | −0.237 |
| 13 | 9 | 280.6 | 22.0 | 41 | 29 | 7.2 | 8.6 | 101.1 | 68.4 | 40 | 11 | 7.3 | 14.0 | 1.036 | −0.048 |
| 14 | 6 | 86.4 | 1.5 | 543 | 28 | 2.5 | 10.7 | 174.0 | 30.1 | 60 | 2 | 7.4 | 38.6 | 1.030 | −0.248 |
| 15 | 8 | 268.8 | 1.4 | 39 | 10 | 7.9 | 15.6 | 158.1 | 56.6 | 22 | 2 | 10.4 | 30.8 | 1.026 | −0.153 |
| 16 | 8 | 257.6 | 51.4 | 21 | 10 | 10.6 | 15.5 | 126.8 | 31.0 | 20 | 5 | 10.8 | 21.9 | 1.070 | −0.06 |
| 17 | 4 | 260.2 | 1.0 | 1088 | 22 | 2.1 | 14.8 | 183.1 | 33.9 | 17 | 5 | 16.5 | 29.5 | 1.025 | −0.109 |
| 18 | 6 | 261.8 | 11.3 | 14 | 11 | 14.9 | 17.0 | 5.0 | 52.3 | 14 | 2 | 14.8 | 33.3 | 1.045 | −0.426 |
| 19 | 7 | 266.8 | 15.3 | 77 | 37 | 6.0 | 8.6 | 14.9 | 48.0 | 65 | 7 | 6.5 | 19.4 | 1.046 | −0.129 |
| 20 | 6 | 99.6 | 17.3 | 113 | 12 | 5.4 | 16.0 | 231.1 | 69.7 | 64 | 6 | 7.8 | 24.4 | 1.054 | −0.218 |
| 21 | 6 | 68.7 | 1.4 | 959 | 65 | 1.8 | 7.0 | 162.0 | 61.2 | 112 | 20 | 5.4 | 12.6 | 1.060 | −0.297 |
| 22 | 5 | 266.7 | 36.7 | 177 | 18 | 4.7 | 14.7 | 67.7 | 55.5 | 37 | 4 | 10.2 | 29.1 | 1.039 | −0.181 |
| 23 | 6 | 255.5 | 37.2 | 93 | 29 | 5.9 | 10.6 | 130.0 | 35.5 | 80 | 2 | 6.4 | 34.4 | 1.042 | −0.387 |
| 24 | 5 | 82.4 | 3.4 | 179 | 51 | 4.7 | 8.7 | 176.7 | 44.3 | 98 | 4 | 6.3 | 30.0 | 1.035 | −0.21 |
| 25 | 4 | 267.7 | 1.5 | 611 | 18 | 2.8 | 16.1 | 33.0 | 73.4 | 252 | 2 | 4.4 | 48.4 | 1.034 | −0.472 |
| 26 | 4 | 55.6 | 43.6 | 3091 | 22 | 1.3 | 14.8 | 153.1 | 6.8 | 24 | 20 | 14.1 | 15.5 | 1.044 | −0.257 |
| 27 | 5 | 256.8 | 0.9 | 10 | 2 | 19.7 | 37.6 | 171.5 | 42.8 | 6 | 1 | 23.8 | 44.6 | 1.047 | 0.110 |
| 28 | 6 | 256.6 | 13.0 | 398 | 48 | 2.9 | 8.2 | 358.8 | 42.5 | 46 | 4 | 8.4 | 27.1 | 1.044 | −0.183 |
| 29 | 7 | 245.9 | 10.8 | 25 | 9 | 10.5 | 16.5 | 354.9 | 63.6 | 44 | 3 | 7.9 | 28.1 | 1.045 | 0.172 |
| 30 | 6 | 259.0 | 0.1 | 135 | 15 | 4.9 | 14.3 | 356.7 | 68.3 | 54 | 4 | 7.8 | 26.1 | 1.038 | −0.353 |
| 31 | 4 | 57.7 | 47.1 | 2044 | 12 | 1.5 | 19.6 | 286.2 | 31.1 | 45 | 12 | 10.4 | 19.5 | 1.041 | −0.425 |
| 32 | 5 | 75.6 | 19.3 | 197 | 15 | 4.4 | 15.8 | 168.0 | 19.2 | 15 | 2 | 15.8 | 43.9 | 1.055 | −0.581 |
| 33 | 5 | 82.4 | 13.8 | 47 | 13 | 9.1 | 17.3 | 196.1 | 49.8 | 42 | 2 | 9.6 | 40.1 | 1.065 | 0.022 |
| 34 | 5 | 251.8 | 6.7 | 64 | 61 | 7.8 | 8.0 | 347.3 | 42.4 | 38 | 3 | 10.1 | 32.0 | 1.038 | −0.334 |
| 35 | 5 | 234.7 | 28.5 | 101 | 14 | 6.2 | 16.5 | 44.3 | 59.2 | 201 | 2 | 4.4 | 40.9 | 1.019 | −0.239 |
| 36 | 6 | 258.0 | 8.3 | 296 | 38 | 3.3 | 9.2 | 354.1 | 12.2 | 66 | 2 | 7.0 | 39.8 | 1.030 | −0.157 |
| 37 | 7 | 249.6 | 23.9 | 123 | 19 | 4.8 | 12.0 | 355.3 | 29.3 | 55 | 5 | 7.0 | 21.9 | 1.023 | 0.005 |
| 38 | 5 | 248.1 | 21.2 | 184 | 5 | 4.6 | 27.7 | 21.9 | 48.5 | 7 | 2 | 22.2 | 40.2 | 1.021 | −0.520 |
| 39 | 4 | 105.7 | 10.8 | 13 | 3 | 9.2 | 24.3 | 338.2 | 41.7 | 3865 | 4 | 1.3 | 38.6 | 1.022 | −0.196 |
| 40 | 4 | 247.8 | 25.0 | 93 | 22 | 7.2 | 14.8 | 3.8 | 43.1 | 2657 | 49 | 1.4 | 9.9 | 1.031 | 0.484 |
| 41 | 5 | 251.3 | 20.0 | 153 | 19 | 5.1 | 14.0 | 25.6 | 61.5 | 112 | 5 | 5.9 | 27.9 | 1.028 | 0.042 |
| 42 | 6 | 269.1 | 41.6 | 24 | 6 | 11.5 | 21.8 | 38.7 | 36.6 | 34 | 12 | 10.6 | 17.4 | 1.018 | 0.323 |
| 43 | 4 | 254.4 | 18.0 | 60 | 16 | 9.0 | 17.4 | 2.9 | 31.3 | 13 | 6 | 15.4 | 22.8 | 1.016 | 0.100 |
| 44 | 5 | 225.7 | 51.0 | 16 | 1 | 15.5 | 47.6 | 5.0 | 29.3 | 21 | 8 | 15.3 | 23.7 | 1.018 | 0.031 |
| 45 | 6 | 266.9 | 13.6 | 44 | 21 | 9.4 | 13.4 | 141.6 | 61.0 | 1769 | 67 | 1.7 | 8.5 | 1.047 | 0.226 |
| 46 | 7 | 263.5 | 2.9 | 76 | 38 | 6.0 | 8.5 | 158.3 | 74.6 | 59 | 10 | 6.9 | 16.3 | 1.030 | −0.146 |
| 47 | 4 | 281.3 | 26.0 | 76 | 19 | 8.0 | 15.9 | 19.1 | 27.7 | 36 | 2 | 11.7 | 41.1 | 1.018 | 0.109 |
| 48 | 7 | 259.5 | 29.5 | 36 | 11 | 9.4 | 16.8 | 101.5 | 26.6 | 19 | 2 | 13.0 | 38.2 | 1.024 | −0.309 |
| 49 | 7 | 273.1 | 4.1 | 154 | 2 | 4.3 | 34.0 | 165.6 | 67.8 | 9 | 5 | 17.3 | 23.6 | 1.018 | 0.057 |
| 50 | 6 | 105.4 | 4.5 | 31 | 3 | 10.1 | 30.7 | 8.2 | 34.5 | 33 | 9 | 12.1 | 22.9 | 1.036 | 0.405 |
| 51 | 6 | 261.7 | 63.5 | 10 | 6 | 17.7 | 23.1 | 70.0 | 21.5 | 12 | 4 | 16.0 | 27.9 | 1.055 | 0.064 |
| 52 | 7 | 292.9 | 42.2 | 41 | 3 | 8.9 | 31.5 | 75.5 | 47.3 | 66 | 8 | 7.0 | 19.2 | 1.018 | 0.502 |
| 53 | 4 | 296.0 | 25.2 | 6 | 3 | 26.8 | 35.9 | 67.2 | 58.2 | 16 | 3 | 17.3 | 38.2 | 1.018 | 0.003 |
| 54 | 6 | 263.5 | 7.7 | 6 | 2 | 22.9 | 33.4 | 167.9 | 31.2 | 18 | 5 | 16.2 | 30.2 | 1.017 | −0.053 |
| 55 | 6 | 206.9 | 3.0 | 26 | 2 | 12.2 | 40.4 | 93.5 | 52.1 | 21 | 5 | 13.5 | 25.6 | 1.036 | 0.335 |
| 56 | 5 | 270.8 | 39.4 | 44 | 8 | 10.5 | 23.4 | 84.8 | 48.8 | 58 | 2 | 8.2 | 42.1 | 1.046 | 0.179 |

* $P = \exp\{2[(\ln K_{max} - \ln K_{mean})^2 + (\ln K_{int} - \ln K_{mean})^2 + (\ln K_{min} - \ln K_{mean})^2]\}^{1/2}$ with $K_{mean} = (K_{max} + K_{int} + K_{min})/3$; Jelinek (1981).
† $T = [2 \ln(K_{int}/K_{min})/\ln(K_{max}/K_{min})] - 1$; Jelinek (1981); Hrouda (1982).

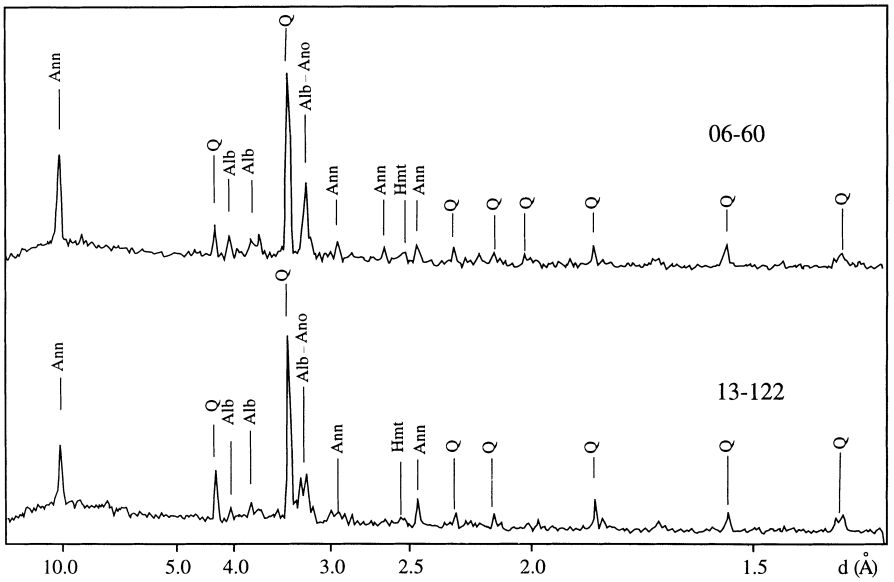


**Figure 4.** Representative spectra of X-ray diffraction of powder of porphyritic monzonite with the interpretation of mineral composition. Q: Quartz, Alb: Albite; Ann: Annite, Ano: Anorthite; Hmt: Hematite.

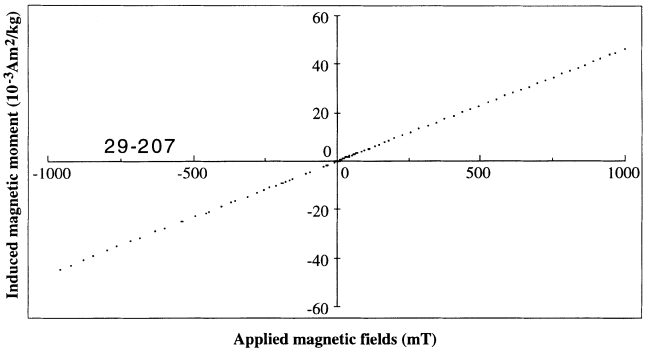


**Figure 5.** Hysteresis curve showing linear and superposing induced magnetic moments with respect to increasing and decreasing applied magnetic fields.

faults, such as the Villefort and Cévennes faults (Fig. 1), the Pont-de-Montvert–Borne pluton probably did not experience any severe internal deformation after its emplacement. This conclusion allows the two massifs to be reconstructed to their initial relative position as a single pluton (Figs 9 and 10). Moreover, for a given locality, the AMS characteristics of the enclaves are indistinguishable from their monzonitic host rock (Fig. 7). The same conclusion applies to the leucogranitic aplitic joints. These observations demonstrate that the porphyritic monzonite, enclaves and aplite dykes all experienced the same deformation under the same tectonic system. Magmatic flow can hardly account for the development of the anisotropy of magnetic susceptibility, which was therefore acquired in the subsolidus stage after a significant amount of crystallization of the monzonite. Furthermore, the consistency of AMS orientations between the monzonite and aplitic joints indicates that the emplacement of granite and the intrusion of dykes are contemporary, as also suggested by their petrographic similarity.

The lineation and foliation orientations of each site are shown in Fig. 9. An E–W-trending lineation is well developed throughout the pluton (Fig. 9a). Planar deformation is more important in the west, especially where the pluton is surrounded by non-porphyritic peraluminous granite (Fig. 9b). The foliation planes generally dip away from the pluton and dip more steeply along the southern border than along the northern one (Fig. 9b). The map of the shape parameter ($T$) shows the distribution of linear and planar magnetic fabrics in the study area (Fig. 10a). As observed in Figs 7, 9 and 10(a),

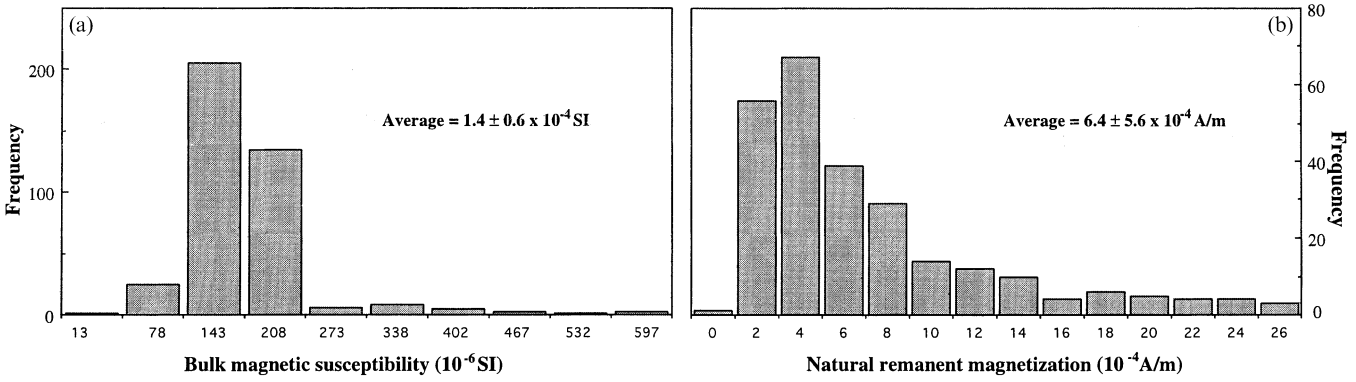


**Figure 6.** Frequency histograms for (a) bulk magnetic susceptibility and (b) natural remanent magnetization.

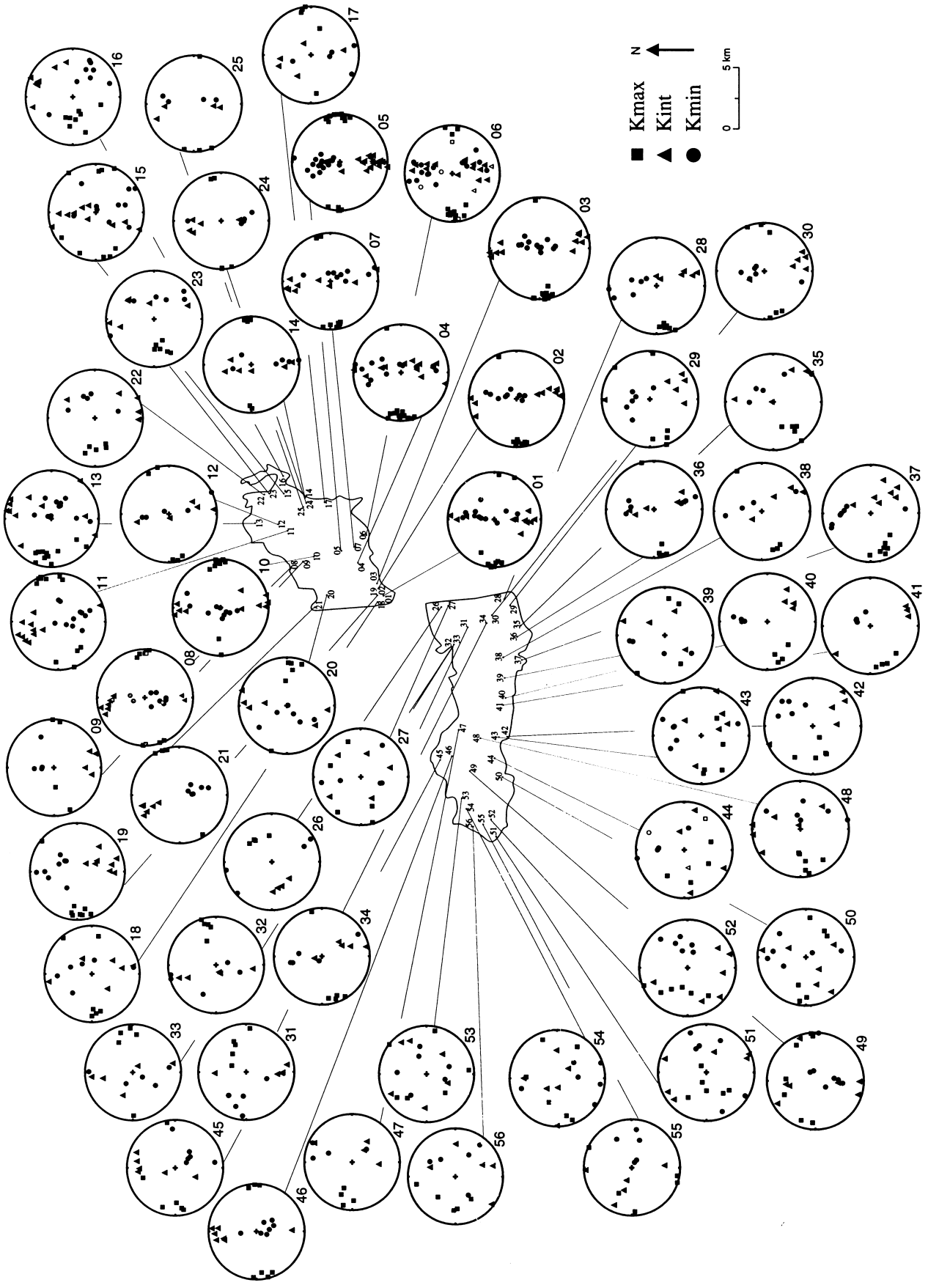


**Figure 7.** Equal-area projection of the directions of magnetic susceptibility principal axes for 56 sites with their geographical position. Squares, triangles and circles represent the $K_{max}$, $K_{int}$ and $K_{min}$ principal axes, respectively. Solid, open and grey symbols correspond to monzonite, enclave and aplite, respectively.

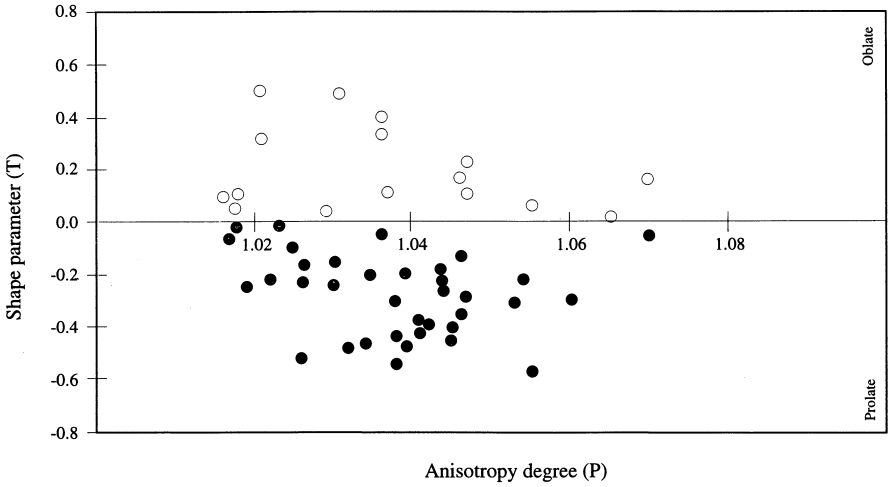


**Figure 8.** Plots of the shape ($T$) and anisotropy degree ($P$) parameters showing low deformation degree and dominant linear deformation. Solid and open symbols indicate linear (prolate) and planar (oblate) shapes, respectively. See Table 1 for the calculations.

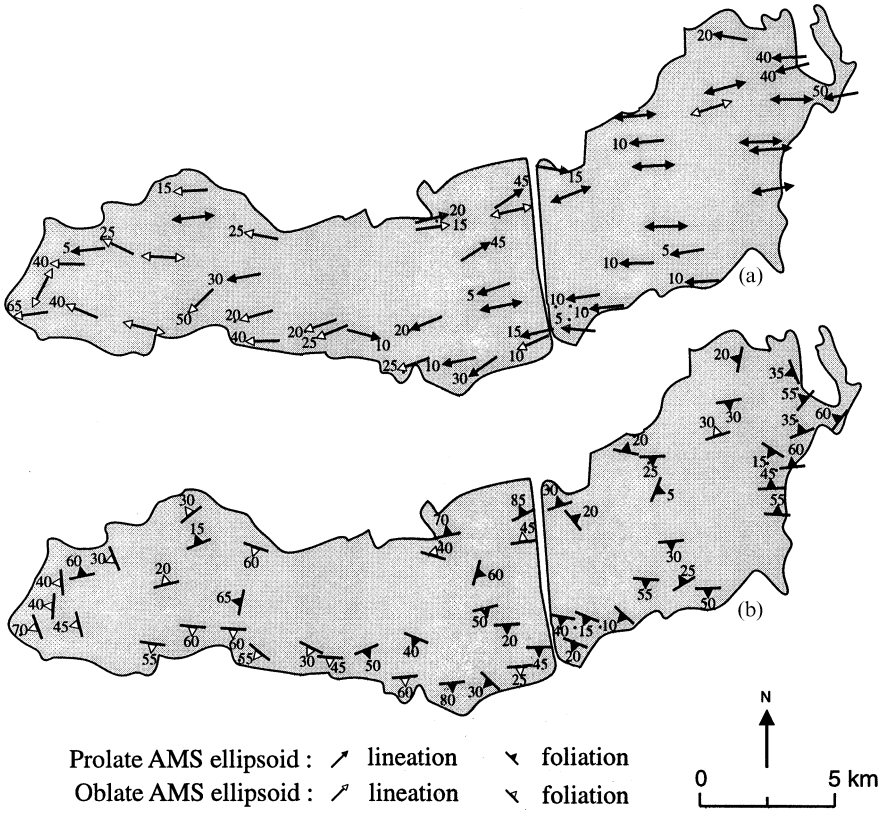


**Figure 9.** Magnetic fabric maps of Pont-de-Montvert–Borne pluton restored to its initial shape before left-lateral displacement along the Villefort fault. (a) magnetic lineation with plunge angle and (b) magnetic foliation with dip angle. For a given site, a solid or open symbol indicates the dominance of linear or planar deformation, respectively.

linear fabric dominates the Borne pluton while the planar one is more important along the southern and southwestern borders in the Pont-de-Montvert pluton. Fig. 10(b) shows that the anisotropy magnitude ($P$ parameter) is heterogeneous at the pluton scale. In general, the $P$ parameter is higher where the linear fabric is dominant and lower where the planar deformation is dominant. The heterogeneity of this $P$ parameter may be due to different types of contacts between igneous and country rocks. The stronger linear deformation is often located in zones where the porphyritic monzonite is in direct contact with micaschists. Conversely, in zones where the porphyritic monzonite is in contact with non-porphyritic peraluminous granite, the planar fabric predominates (Fig. 10).

As a whole, the planar and linear patterns are in good agreement with granite fabric inferred from mineral preferred AMS orientation (Faure *et al.* 1992). The well-marked E–W linear fabric shown by stretched enclaves and N–S-trending aplitic joints (Fig. 1) is also well recognized in the magnetic

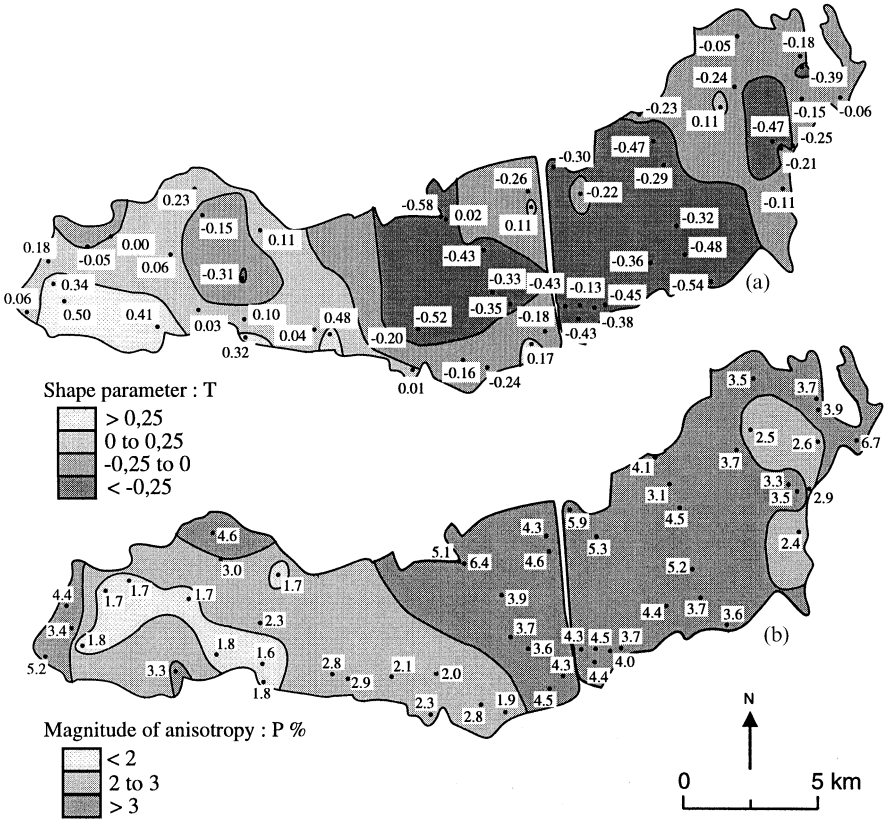


**Figure 10.** Maps of anisotropy parameters of the Pont-de-Montvert–Borne pluton. (a) shape parameter $T$; (b) magnitude of anisotropy, $P$, in per cent.

fabric. Recent gravity investigations in the Mont Lozère area (Marthelet *et al.* 1999) show that the most important negative gravity anomaly is located in the west corner of the Pont-de-Montvert–Borne pluton, which is interpreted as the granite root. Moreover, the anomaly gradient is steeper along the southern border than along the northern one. This observation is in agreement with the foliation dip pattern, namely steep in the south and gentle in the north (Fig. 9b). The intrusion was almost horizontally eastwards, as shown by the E–W-stretching lineation with low dip angle (Fig. 9a).

The Hercynian orogenic belt is a Devonian–Carboniferous collision orogen between Gondwana and Laurussia. After the main compression ceased in the Early Carboniferous in the French Massif Central, the tectonics evolved into an E–W extensional regime coincident with the emplacement of numerous granitic plutons (e.g. Faure & Pons 1991; Faure 1995). The structure of the Pont-de-Montvert–Borne pluton inferred from both AMS and mineral fabrics, together with structural analysis of the host rocks and a gravimetric survey, is in agreement with this interpretation.

## ACKNOWLEDGMENTS

This study has been supported by the CNRS-BRGM-Ministère de l'Education Nationale program GEOFRANCE 3D. The authors wish to thank S. Gilder and J. Pons for valuable suggestions for improving the redaction of this paper, as well as M. Le Goff for his help in the laboratory work. The authors are greatly indebted to Professor Tarling and an anonymous reviewer for their critical and constructive reading of the manuscript. This is contribution GEOFRANCE 3D no. 75.

## REFERENCES

Bingham, C., 1964. Distribution on a sphere and on the projective plane, *PhD thesis,* Yale University, New Haven, CT.

Borradaile, G.L., Keeler, W., Alford, C. & Sarvas, P., 1987. Anisotropy of magnetic susceptibility of some metamorphic minerals, *Phys. Earth planet. Inter.,* **48,** 161–166.

Bouchez, J.L., Delas, C., Gleizes, G., Nédélec, A. & Rochette, P., 1990. Microstructure and magnetic susceptibility applied to emplacement kinematics of granites: example of the Foix Pluton (French Pyrenees), *Tectonophysics,* **184,** 157–171.

Caron, C., 1994. Les minéralisations Pb-Zn associées au Paléozoïque inférieur d'Europe méridionale, Traçage isotopique Pb-Pb des gîtes de l'Iglesiente (SW Sardaigne) et des Cévennes, Evolution du socle encaissant par la géochronologie U-PB, Ar-Ar et K-Ar, *PhD thesis,* Université de Montpellier, Montpellier.

Charonnat, X., Faure, M. & Chauvet, A., 1997. Relationship between Au-Sb mineralization, Mont Lozère granite, Alès coal, basin and Villefort fault (French Massif Central), *Euro. Un. Geosc.,* **9,** 547 (abstract).

Ellwood, B.B. & Wenner, D.B., 1981. Correlation of magnetic susceptibility with $^{18}O$: $^{16}O$ data in orogenic granites of the southern Appalachian Piedmont, *Earth Planet. Sci. Lett.,* **59,** 200–202.

Ellwood, B.B. & Whitney, J.A., 1980. Magnetic fabric of the Elberton granite, Northeast Georgia, *J. geophys. Res.,* **85,** 1481–1486.

Faure, M., 1995. Late orogenic Carboniferous extensions in the Variscan French Massif Central, *Tectonics,* **14,** 132–153.

Faure, M. & Pons, J., 1991. Crustal thinning recorded by the shape of the Namurian–Westphalian leucogranite in the Variscan belt of the Northwest Massif Central, France, *Geology,* **19,** 730–733.

Faure, M., Pons, J. & Babinault, J.-F., 1992. Le pluton du Pont-de-Montvert: un granite syntectonique entravasé vers l'Est pendant le désépaississement crustal varisque du Massif Central français, *C. R. Acad. Sci. Paris,* **315,** 201–208.

Faure, M., Charonnat, X. & Chauvet, A., 1999. Schéma structural et évolution tectonique du domaine para-autochtone cévenol de la chaîne hercynienne (Massif Central français), *C. R. Acad. Sci. Paris,* **328,** 401–407.

Fernandez, A., 1977. Sur la structure et la mise en place du granite porphyroïde du Pont-de-Montvert (Mont Lozère, Massif Central français), *C. R. Som. Soc. géol. France,* **3,** 137–140.

Graham, J.W., 1954. Magnetic susceptibility anisotropy, an unexploited petrofabric element, *Geol. Soc. Am. Bull.,* **65,** 1257–1258.

Hargraves, R.B., Johnson, D. & Chan, C.Y., 1991. Distribution anisotropy: the cause of AMS in igneous rocks? *Geophys. Res. Lett.,* **18,** 2193–2196.

Hrouda, F., 1982. Magnetic anisotropy of rocks and its application in geology and geophysics, *Geophys. Surv.,* **5,** 37–82.

Hrouda, F. & Chlupacova, M., 1980. The magnetic fabric in the Nasavrky Massif, *Cas Mineral. Geol.,* **25,** 17–27.

Jelinek, V., 1981. Characterization of the magnetic fabric of rocks. *Tectonophysics,* **79,** 563–567.

Khan, M.A., 1962. The anisotropy of magnetic susceptibility of some igneous and metamorphic rocks, *J. geophys. Res.,* **67,** 2873–2885.

King, R.F., 1966. The magnetic fabric of some Irish granites, *Geol. J.,* **5,** 43–66.

Marre, J., 1982. *Méthode d'analyse Structurale des Granitoïdes,* Bureau de Recherches géologiques et Minières, Orléans.

Marthelet, G., Diament, M. & Truffert, C., 1999. Un levé gravimétrique détaillé dans le Cévennes: apport à l'imagerie crustale (programme GéoFrance 3D—Massif central), *C. R. Acad. Sci. Paris,* **328,** 727–732.

Mattauer, M. & Etchecopar, A., 1976. Argumentation en faveur de chevauchements de type himalayen dans la chaîne hercynienne du Massif Central français, *Coll. Int. CNRS,* **268,** 261–267.

Matte, P., 1986. La chaîne varisque parmi les chaînes paléozoïques péri-atlantiques, modèle d'évolution et position des grands blocs continentaux au Permo-Carbonifère, *Bull. Soc. Géol. France,* **8,** 9–24.

Mialhe, J., 1980. Le massif granitique de la Borne (Cévennes), étude pétrographique, géochimique, géochronologique et structurale, *PhD thesis,* University of Clermont-Ferrand.

Monié, P., Bouchot, V., Faure, M., Charonnat, X. & Najoui, K., 1999. $^{39}Ar/^{40}Ar$ laser-probe dating of W-Au-Sb deposits in the southern French massif Central (Cévennes and Châtaigneraie), *Eur. Un. Geosci.,* **10,** 477 (abstract).

Rakib, A., 1996. Le métamorphisme régional de basse pression des Cévennes occidentales: une conséquence directe de la mise en place du dôme thermique vellave (Massif Central français), *PhD thesis,* Université de Montpellier, Montpellier.

Rochette, P., Jackson, M. & Aubourg, C., 1992. Rock magnetism and the interpretation of anisotropy of magnetic susceptibility, *Rev. Geophys.,* **30,** 209–226.

Tarling, D.H. & Hrouda, F., 1993. *The Magnetic Anisotropy of Rocks,* Chapman & Hall, London.

Van Moort, J.C., 1966. Les roches cristallophylliennes des Cévennes et les roches plutoniques du Mont Lozère, *Ann. Fac. Sci. Clermont-Ferrand,* **31** (14), 1–272.

Zapletal, K., 1990. Low-field susceptibility anisotropy of some biotite crystals, *Phys. Earth planet. Inter.,* **63,** 85–97.